

Star formation and fractal properties of the interstellar medium: a study of Hi-GAL observations of the third Galactic quadrant

Davide Elia - 1. INAF-IAPS Rome (Italy)



F. Strafella², N. Schneider³, R. Paladini⁴, R. Vavrek⁵, S. Molinari¹, S. Pezzuto¹, A. Noriega-Crespo⁶, A. M. Di Giorgio¹, A. Traficante⁷, K. Rygl⁸, E. Schisano^{1,4}, P. Natoli⁹, P. Martin¹⁰, Y. Fukui¹¹

2. Università del Salento, Lecce, Italy – 3. Univ. Bordeaux, LAB, CNRS, France – 4. California Institute of Technology, Pasadena, USA – 5. European Space Astronomy Centre, Spain – 6. Space Telescope Science Institute, Baltimore, USA – 7. Jodrell Bank Centre for Astrophysics, Manchester, UK – 8. ESA-ESTEC, Noordwijk, The Netherlands – 9. Università di Ferrara, Italy – 10. Canadian Institute for Theoretical Astrophysics, Toronto, Canada – 11. Nagoya University, Japan

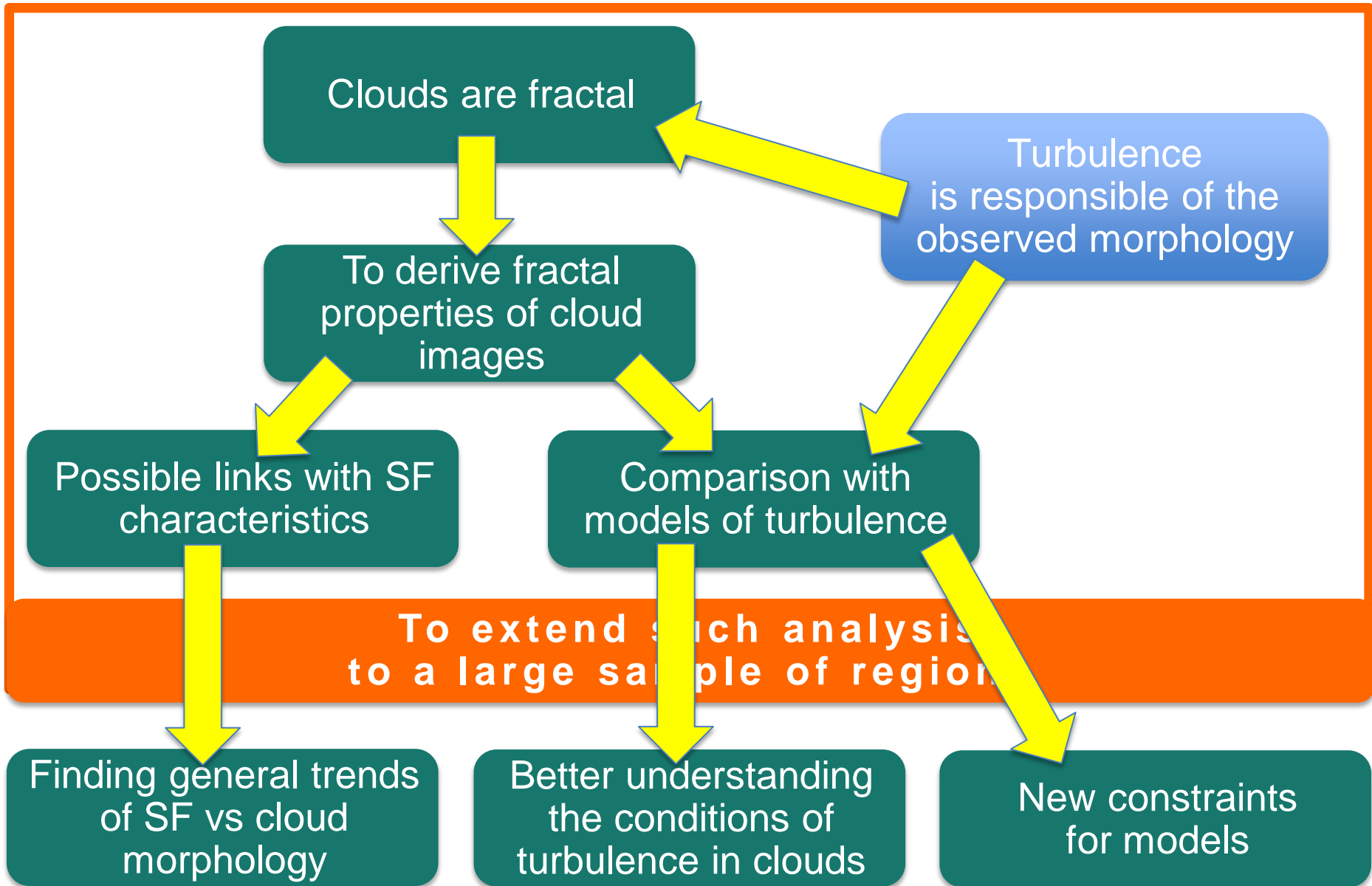
CLOUDS AND FRACTALS



Clouds are not spheres, mountains are not cones,
coastlines are not circles, and bark is not smooth,
nor does lightning travel in a straight line.

(Benoit Mandelbrot)

CONCEPTUAL FRAMEWORK



CHARACTERIZING THE STRUCTURE OF DIFFUSE EMISSION IN HI-GAL MAPS

D. ELIA¹, F. STRAFELLA², N. SCHNEIDER³, R. PALAZZI⁴, R. VAVREK⁵, S. MARUCCIA², S. MOLINARI¹, A. NORIEGA-CRESPO^{4,6},
S. PEZZUTO^{4,5}, K. L. J. RYGL^{1,7}, A. M. DI GIORGIO¹, A. TRAFICANTE⁸, E. S. CASANO⁴, L. CALZOLETTI⁹, M. PESTALOZZI¹,
S. J. LIU¹, P. NATOLI^{9,10,11}, M. HUANG¹³, P. MARTIN¹⁴, Y. FUJITA¹⁵, AND T. HAYAKAWA¹⁵

¹ INAF-IAPS, Via Fosso del Cavaliere 100, I-00133 Roma, Italy; davide.elia@iaps.inaf.it

² Dipartimento di Matematica e Fisica E. De Giorgi, Università del Salento, CP 311, I-73100 Lecce, Italy

³ Univ. Bordeaux, CNRS, UMR 5804, F-33070, Floirac, France

⁴ Space Telescope Science Institute, 3700 San Martin Drive, Baltimore, MD 21218, USA

⁵ Infrared Processing and Analysis Center, California Institute of Technology, Pasadena, CA 91125, USA

⁶ Herschel Science Centre, European Space Astronomy Centre, Villafranca del Castillo, Madrid, Spain

⁷ Research and Scientific Support Department, European Space Agency, Noordwijk, The Netherlands

⁸ Jodrell Bank Centre for Astrophysics, Manchester, UK

⁹ Agenzia Spaziale Italiana, Bologna, Italy

¹⁰ Dipartimento di Fisica, Università di Ferrara, Ferrara, Italy

¹¹ Dipartimento di Astronomia, Università di Padova, Padova, Italy

¹² Dipartimento di Astronomia, Università di Bologna, Bologna, Italy

¹³ National Astronomical Observatories, Chinese Academy of Sciences, Beijing, 100012, China

¹⁴ Canadian Institute for Advanced Study, University of Toronto, 60 St. George Street, Toronto, ON M5S 3H8, Canada

¹⁵ Department of Science, Nagoya University, Furo-cho, Chikusa-ku, Nagoya, 464-8602, Japan

Received 2014 January 17; accepted 2014 April 25; published 2014 May 16

PUBLISHED

SURVEYED AREA



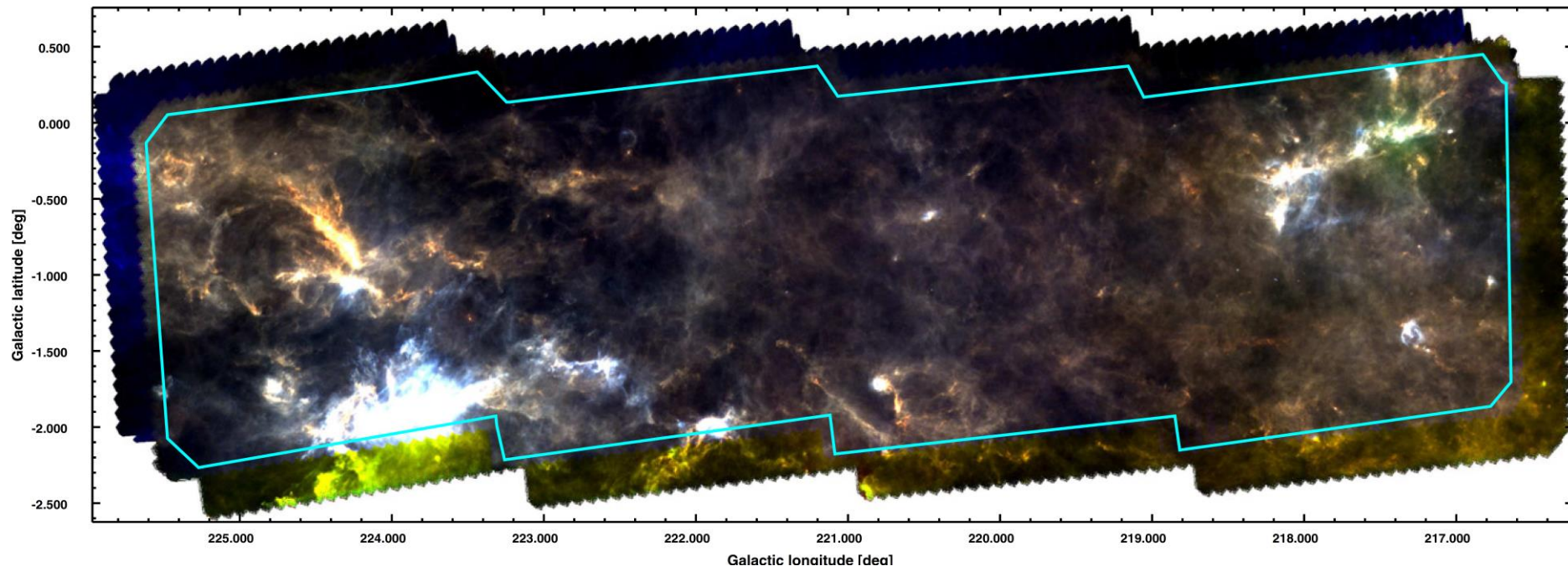
Four $2.3^\circ \times 2.3^\circ$ adjacent tiles in the Galactic 3rd quadrant (Elia+ 2013), namely the first available Hi-GAL observations of the outer Galaxy.

We denote them with $l=217$, $l=220$, $l=222$, and $l=224$, respectively.

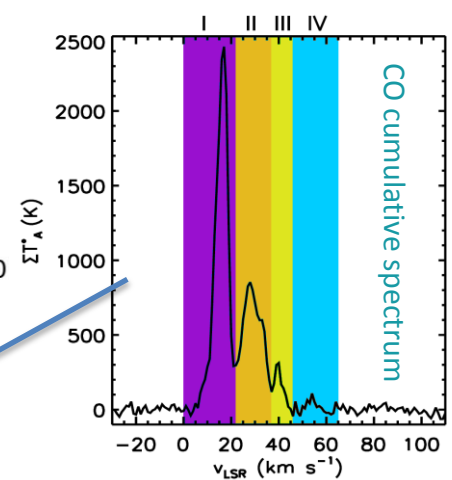
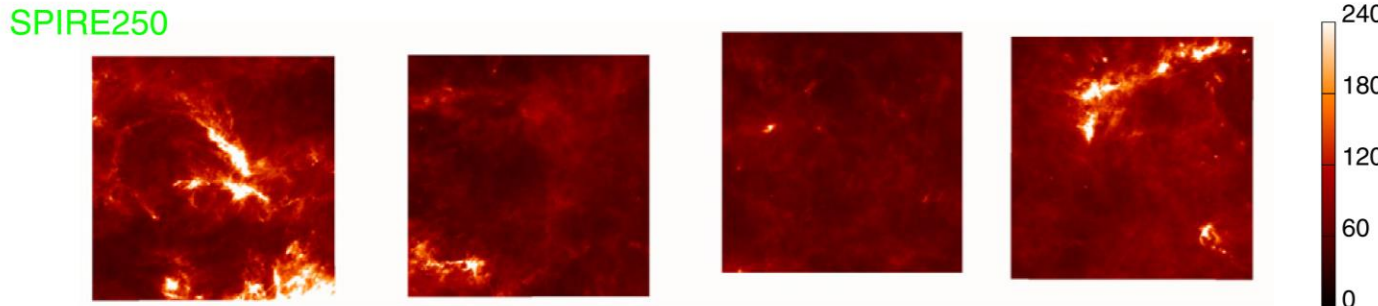
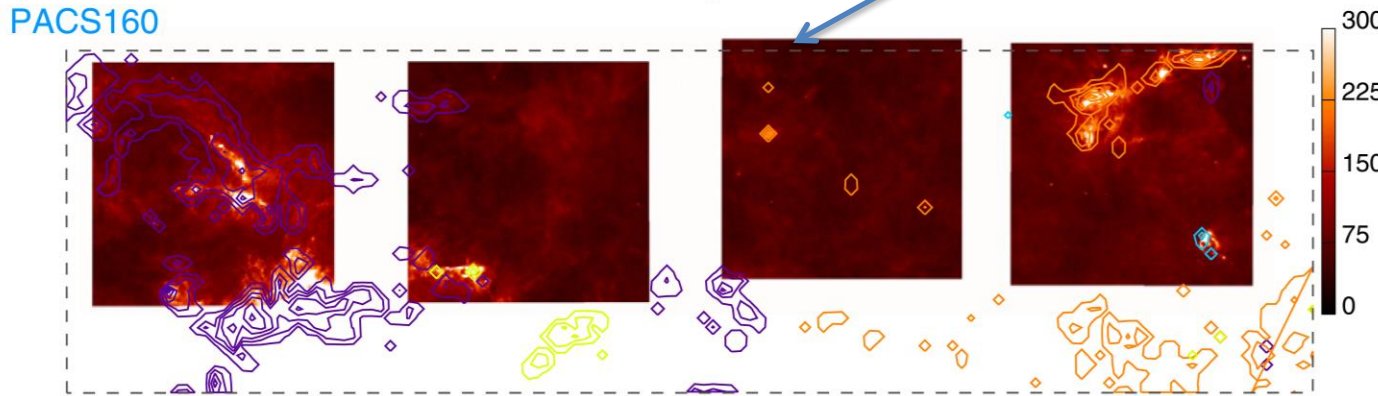
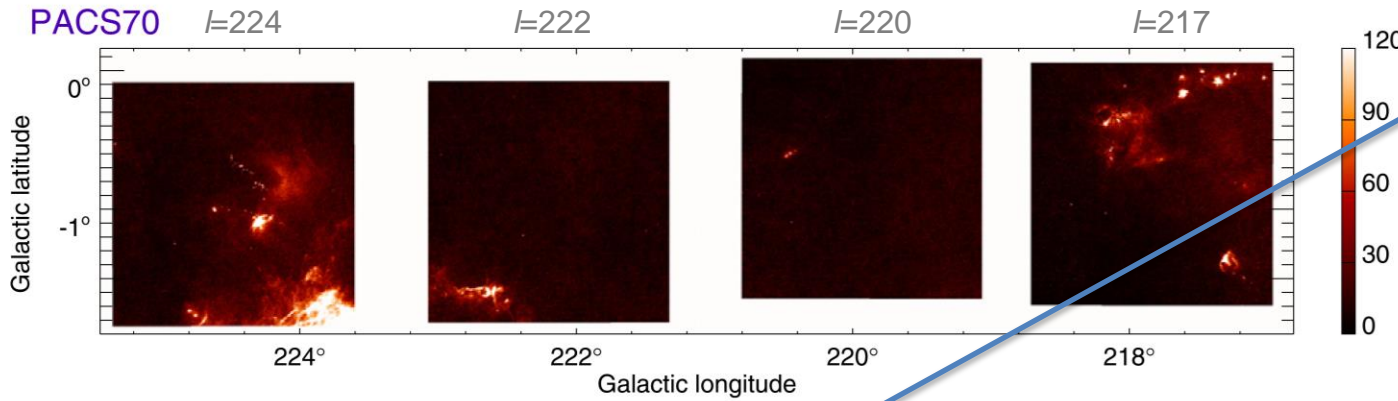
They represent an ideal case for studying the structure of the ISM, for two main reasons:

- 1) The lower occurrence of compact bright sources and star forming regions;
- 2) The lower degree of confusion along the line of sight, testified by CO(1-0) NANTEN maps.

Four main velocity components have been identified, with a very low degree of overlap, located at 1.1 kpc (component I), 2.2 kpc (II), 3.3 kpc (III) and 5.8 kpc (IV), respectively.

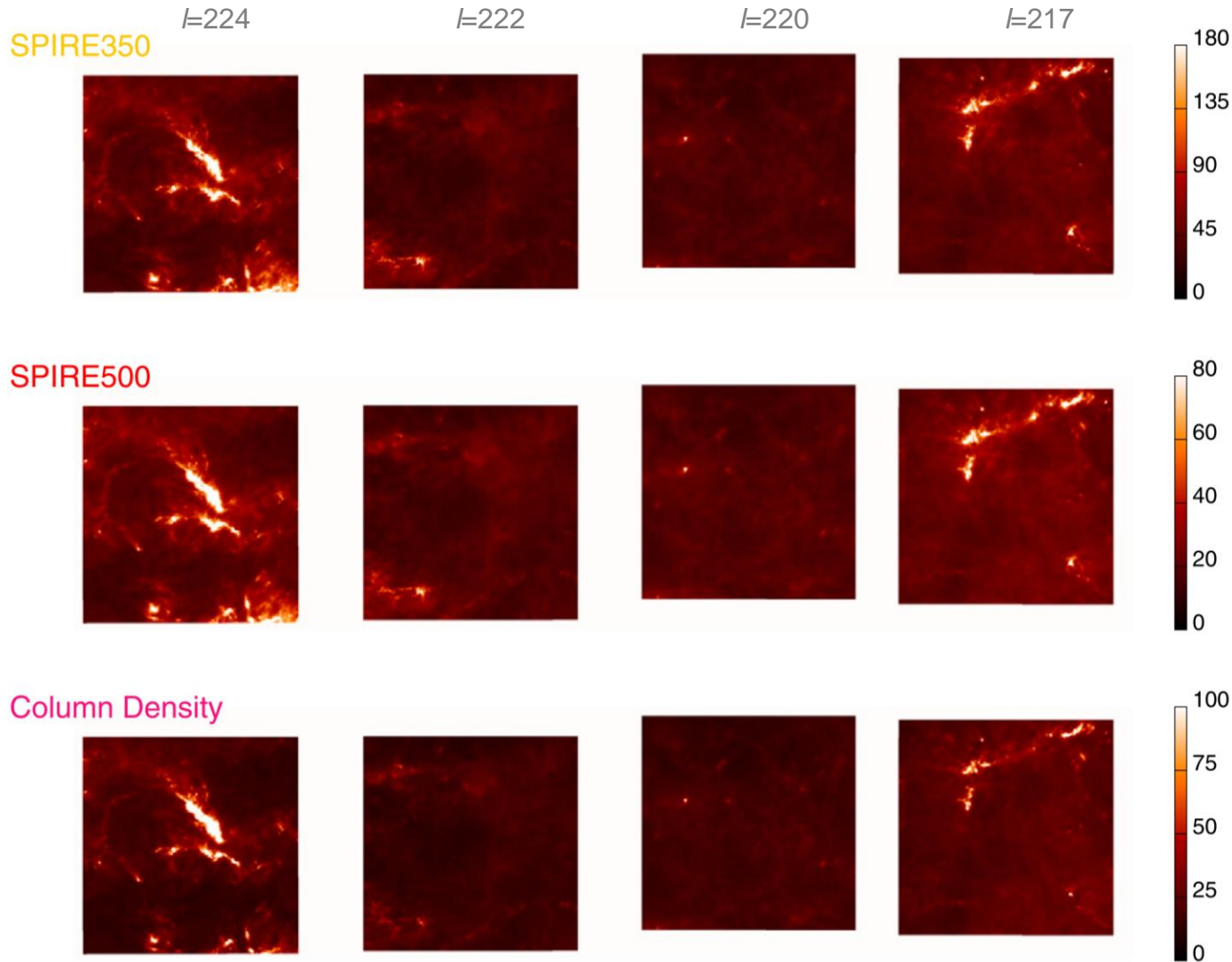


ANALYZED FIELDS - 1



The four investigated Hi-GAL fields, observed at different bands (blue: 70 μm , cyan: 160 μm , green: 250 μm). Color scales are linear. Units are MJy/sr . The NANTEN CO(1-0) contours (Eli $+$. 2013) are overplotted on the 160 μm maps, starting from 5 K km s^{-1} and in steps of 15 K km s^{-1} . Distance components I, II, III, and IV are represented with purple, orange, yellow, and cyan contours, respectively. The area surveyed in CO(1-0) is delimited by a gray dashed line.

ANALYZED FIELDS - 2



As in the previous figure, but for further bands:

orange: 350 μm , red: 500 μm , magenta: column density.

The color scales are linear. The units are MJy sr^{-1} for the SPIRE maps, and 10^{20} cm^{-2} for the column density ones.

The maps of column density have been obtained through a pixel-to-pixel grey-body fit, using the wavelengths from 160 to 500 μm .

POWER SPECTRUM AND fBm SETS

The power spectrum is defined as the square modulus of its own Fourier transform. A convenient approach is to study the shell-averaged power spectrum $P(k)$, where $k = (k_x^2 + k_y^2)^{1/2}$.

Typically a search for a power-law behavior in the spectrum is carried out. The presence of such a power-law behavior can be interpreted as an indication of turbulence (in the Kolmogorov 1941 case, for the 3-D velocity field of incompressible fluids a dependence of $P(k) \propto k^\beta$ is found, with $\beta = -11/3$), and might suggest the characteristic scales at which both energy injection and dissipation take place.

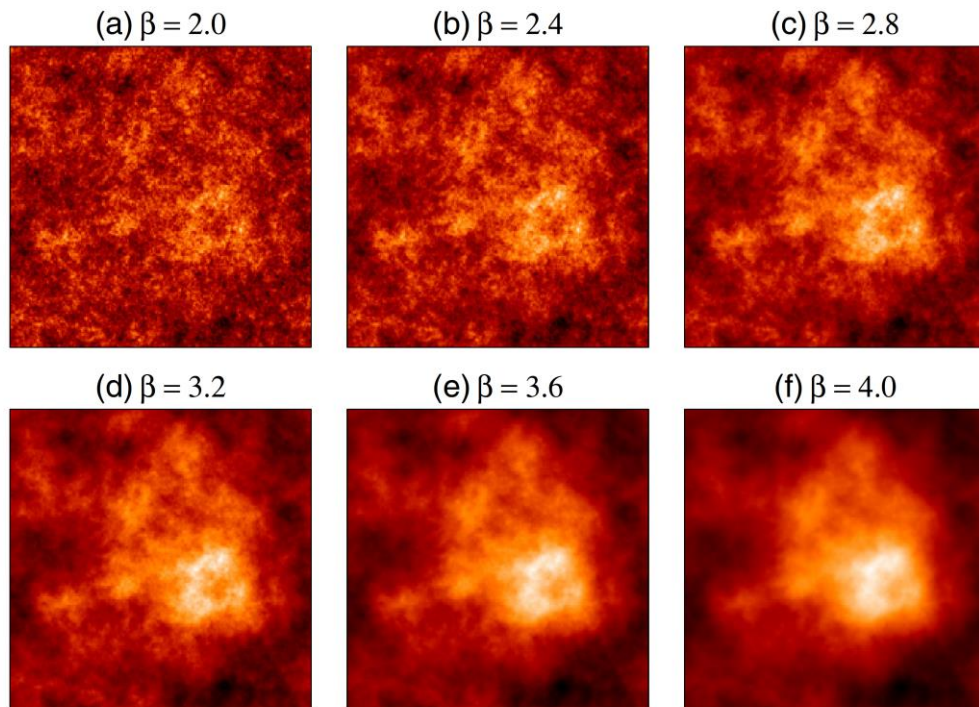
Fractional Brownian motion (fBm) images:

- i) Power-law power spectrum.
- ii) Random phase distribution.

The fBm images are easy to generate, and frequently used as surrogates of the ISM maps. They look increasingly smoother as β increases.

They are fractal images, and the analytic relation between β and the fractal dimension D is

$$D = (8 - \beta) / 2 \quad [1]$$



Δ -VARIANCE TECHNIQUE

Given a two-dimensional observable field $A(x,y)$, and $r=(x^2+y^2)^{1/2}$, a *Mexican hat* filter corresponding to the spatial scale L can be defined as

$$\odot_L(r) = \frac{4}{\pi L^2} e^{-\frac{r^2}{(L/2)^2}} - \frac{4}{\pi L^2(v^2 - 1)} \left[e^{-\frac{r^2}{(vL/2)^2}} - e^{-\frac{r^2}{(L/2)^2}} \right] \quad [2]$$

where the two main terms in the right side of the equation represent the *core* and the *annulus* components, respectively, and v is the diameter ratio between them.

The Δ -variance at the scale L is defined (Stutzki+ 1998) as the variance of the convolution of A with the filter function:

$$\sigma_{\Delta}^2(L) = \frac{1}{2\pi} \left\langle \left(A * \odot_L \right)^2 \right\rangle_{x,y} \quad [3]$$

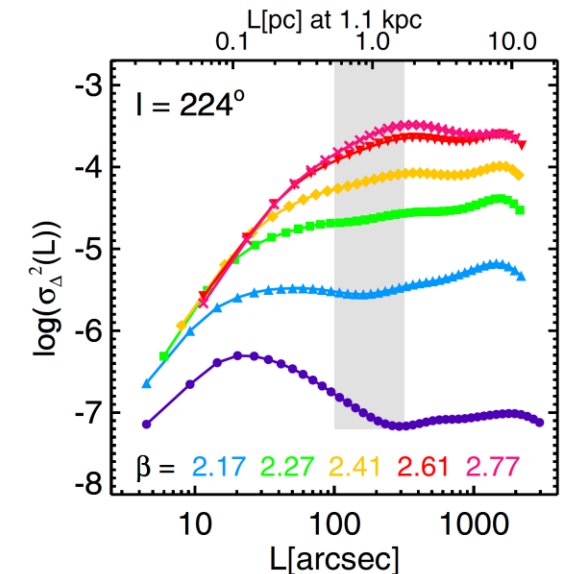
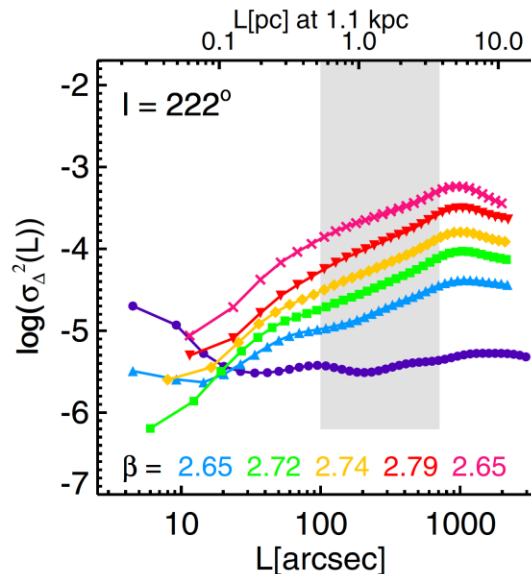
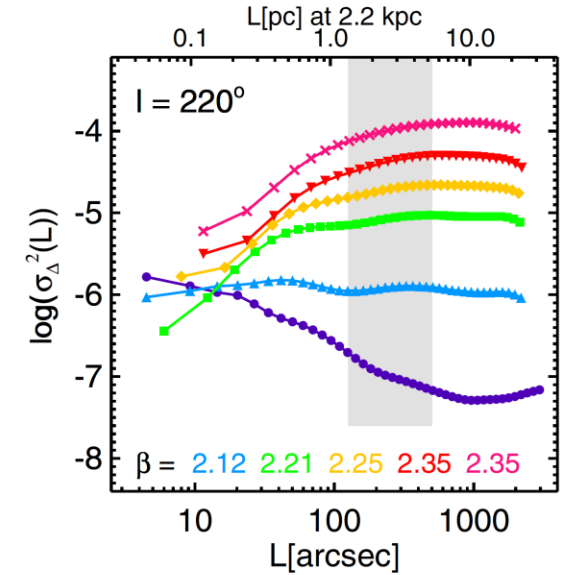
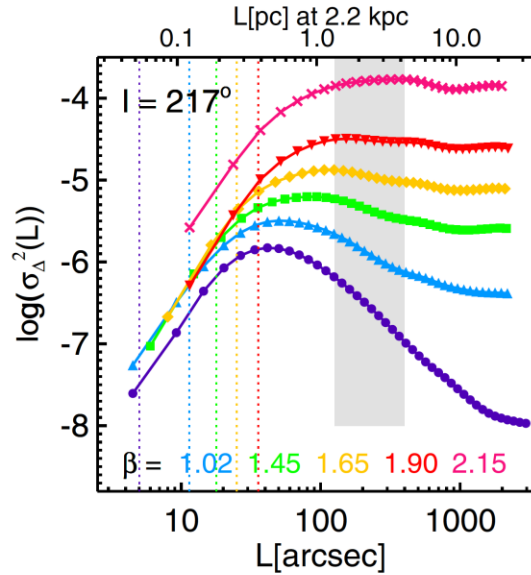
The fundamental relation between the slopes of Δ -variance and of the power spectrum (β) was shown by Stutzki+ 1998:

$$\sigma_{\Delta}^2(L) \propto L^{\beta-2} \quad [4]$$

Δ -VARIANCE OF ANALYZED FIELDS

Δ -variance curves of the analyzed maps, as a function of the spatial scale L . The linearity range is highlighted as a gray area. The corresponding linear slopes are transformed in power spectrum slopes through Equation [1] and reported on the bottom of each panel (except for $70\ \mu\text{m}$). The spatial scales corresponding to the nominal beams at each band are plotted as dotted lines in the top-left panel; scales below them are meaningless.

A systematic increase of the slope with the wavelength is found from 160 to $500\ \mu\text{m}$. At shorter wavelengths the contribution of warmer very small grains seems to be responsible for a more uniform distribution of the power of the image through the different spatial scales (then a shallower β).



FRACTAL DIMENSION AND TURBULENCE

Equation [1] makes it possible to convert the power spectrum exponent β into the corresponding fractal dimension D :

Field	Distance (kpc)	Fit Range (pc)	β					D				
			160 μm	250 μm	350 μm	500 μm	Col. Dens.	160 μm	250 μm	350 μm	500 μm	Col. Dens.
$\ell 217$	2.2	1.3–4.2	1.02	1.45	1.65	1.90	2.15	3.49	3.27	3.17	3.05	2.93
$\ell 220$	2.2	1.3–5.3	2.12	2.21	2.25	2.35	2.35	2.94	2.89	2.87	2.83	2.83
$\ell 222$	1.1	0.5–3.8	2.65	2.72	2.74	2.79	2.65	2.67	2.64	2.63	2.61	2.68
$\ell 224$	1.1	0.5–1.7	2.17	2.27	2.41	2.61	2.77	2.91	2.86	2.79	2.70	2.61

Relevant results:

1. These values of D are far away from the first estimates of two decades ago ($D = 2.3$; Falgarone+ 1991; Elmegreen 1997), and more compatible with the power spectra slopes of compressible turbulence (e.g., Federrath+ 2009).
2. For both distance components, the fractal dimension of the tiles with active star formation ($l=224$, $l=217$) is larger than in the quiescent ones ($l=222$, $l=220$).

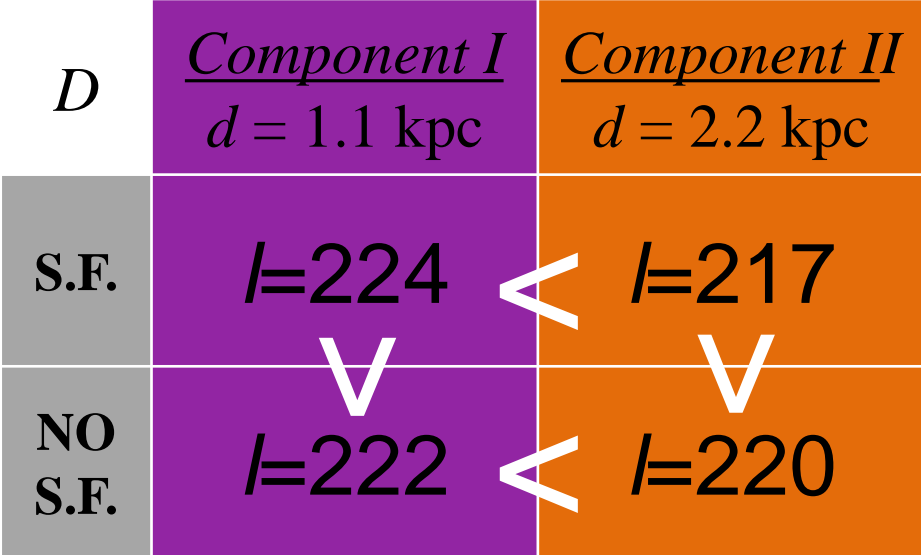
FRACTAL DIMENSION AND TURBULENCE

Field	Distance (kpc)	Fit Range (pc)	β					D				
			160 μm	250 μm	350 μm	500 μm	Col. Dens.	160 μm	250 μm	350 μm	500 μm	Col. Dens.
$\ell 217$	2.2	1.3–4.2	1.02	1.45	1.65	1.90	2.15	3.49	3.27	3.17	3.05	2.93
$\ell 220$	2.2	1.3–5.3	2.12	2.21	2.25	2.35	2.35	2.94	2.89	2.87	2.83	2.83
$\ell 222$	1.1	0.5–3.8	2.65	2.72	2.74	2.79	2.65	2.67	2.64	2.63	2.61	2.68
$\ell 224$	1.1	0.5–1.7	2.17	2.27	2.41	2.61	2.77	2.91	2.86	2.79	2.70	2.61

Relevant results:

3. The **Component I** tiles show smaller values of D compared with the corresponding **Component II** ones. If turbulence is responsible of that (more turbulence produces larger D , e.g. Kritsuk+ 2006) a lower star formation efficiency (e.g., Gazol & Kim, 2010) in **Component II** should be expected. This has been found, in fact, by Elia+ (2013):

$SFE_I=0.008$ and $SFE_{II}=0.004$, respectively.



CLUMP MASS FUNCTION

For a fBm-like cloud (with power spectrum slope β), assuming

- clump mass spectrum in the cloud $dN/dM \propto M^{-\alpha}$
 - clump mass vs size as $M \propto r^\gamma$,
- the following relation is expected:

$$\beta = (3 - \alpha)\gamma \quad [5] \quad \text{Stutzki+ (1998)}$$

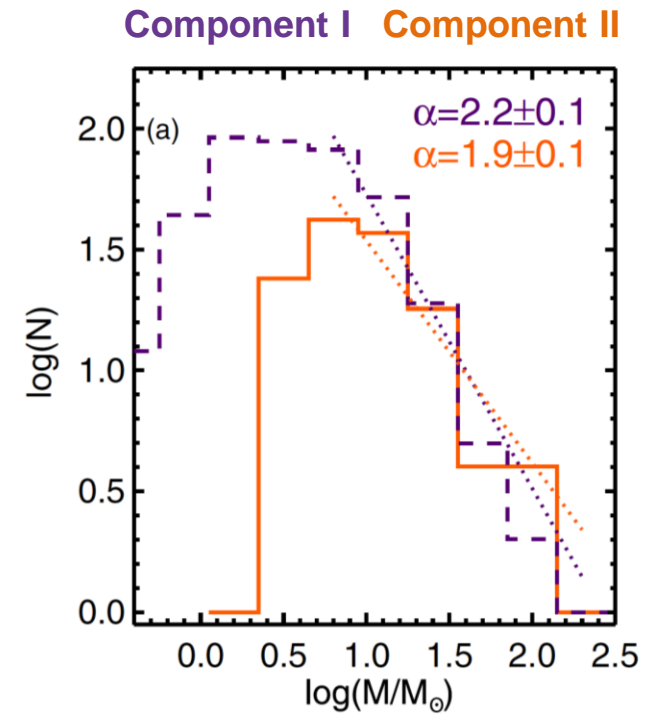
A first test of Equation [5] is possible:

- α from Elia+ (2013);
- β from the column density power spectrum slope of the two quiescent fields ($l=222$ for **Component I** and $l=220$ for **Component II**, respectively).

We find $\gamma_I=3.4\pm0.2$ and $\gamma_{II}=2.2\pm0.1$.

However, both components don't show an evident power-law behavior, but rather a high degree of dispersion.

The γ value obtained for **Component II** looks more meaningful from the physical point of view, probably because this population is entirely composed by clumps, the kind of structures Eq. [5] refers to.



CONCLUSIONS

1. *The analyzed maps (160–500 μm + column density) show common features of the Δ -variance, i.e. spatial scales corresponding to peaks and turn-over points. However, the power spectrum slope changes, generally increasing from 160 μm to 500 μm , probably due to a different spatial displacement of small against large grain dust components.*
2. *The power spectrum slopes vary from tile to tile: the power spectrum and the fractal dimension of the ISM are far from being constant and universal.*
3. *None of these slopes are consistent with the Kolmogorov's incompressible turbulence. The model of supersonic isothermal turbulence of Federrath+ (2009) seems more realistic.*
4. *The power spectrum slopes of the two eastern fields ($d = 1.1$ kpc), are steeper than those of the western fields ($d = 2.2$ kpc). This suggests a higher degree of turbulence in the latter distance component, compatible with the observed lower star formation efficiency. This represents an interesting evidence of the connection, predicted by the theory, between fractality and star formation efficiency.*